

I-Scene: 3D Instance Models are Implicit Generalizable Spatial Learners

Lu Ling^{1*}, Yunhao Ge², Yichen Sheng², Aniket Bera¹,
¹Purdue University ²NVIDIA Research

[I-Scene Project Page](#)

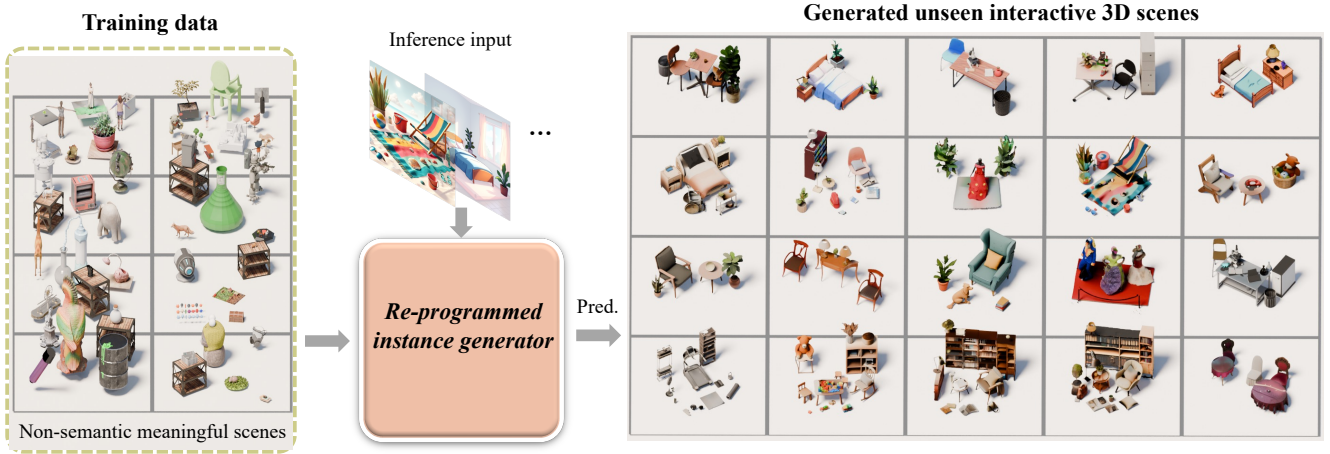


Figure 1. A pre-trained 3D instance model is re-programmed into a scene-level spatial learner. It learns spatial priors from non-semantic scenes (randomly composed instances) in a feed-forward manner, producing coherent layouts and unseen interactive 3D scenes.

Abstract

Generalization remains the central challenge for interactive 3D scene generation. Existing learning-based approaches ground spatial understanding in limited scene dataset, restricting generalization to new layouts. We instead reprogram a pre-trained 3D instance generator to act as a scene-level learner, replacing dataset-bounded supervision with model-centric spatial supervision. This reprogramming unlocks the generator’s transferable spatial knowledge, enabling generalization to unseen layouts and novel object compositions. Remarkably, spatial reasoning still emerges even when the training scenes are randomly composed objects. This demonstrates that the generator’s transferable scene prior provides a rich learning signal for inferring proximity, support, and symmetry from purely geometric cues. Replacing widely used canonical space, we instantiate this insight with a view-centric formulation of the scene space, yielding a fully feed-forward, generalizable scene generator that learns spatial relations directly

from the instance model. Quantitative and qualitative results show that a 3D instance generator is an implicit spatial learner and reasoner, pointing toward foundation models for interactive 3D scene understanding and generation. The code is accessible at [the project page](#).

1. Introduction

Generalization remains the central obstacle to interactive 3D scene generation. An effective system must produce editable, affordance-aware, and spatially coherent object arrangements, capabilities critical for virtual content creation, simulation, and embodied AI. Recent end-to-end approaches extend powerful image-to-3D *instance* priors [21, 23] to multiple objects and relations in a single pass, yet their spatial understanding is typically learned from curated scene datasets whose limited coverage does not scale and ultimately constrains generalization to new layouts.

Recent methods learn layouts directly from annotated scenes [8, 17, 20, 24]; for example, SceneGen [17] explicitly models poses on 3D-FRONT [5], and MIDI [8]

*Corresponding author.

learns inter-object relations from those annotations. However, available interactive scene datasets are limited in scale, diversity, and spatial variety. For instance, the widely used interactive 3D scene dataset 3D-FRONT contains only $\sim 20\text{K}$ indoor bedroom and living-room scenes and under-represents small and supporting objects. Consequently, scene layout-supervised models often *overfit to dataset-specific biases* and fail to generalize to broader scene distributions—for example, small objects placed on or behind large furniture or outdoor settings.

Our key insight is that a pre-trained 3D instance model implicitly encodes transferable spatial knowledge—depth, occlusion, scale, and support—even though it outputs single-mesh geometry. We *reprogram* this prior as a scene-level spatial learner to provide model-centric spatial supervision and enables it generalize to unseen layouts, eliminating dependence on curated scene annotations.

A key obstacle to turning an instance generator into a scene-level learner is that its canonical object space suppresses spatial sensitivity: different views are collapsed into the same canonical representation, destroying layout cues needed for scene reasoning. To overcome this limitation, we replace the widely used canonical space with a view-centric scene space, in which each scene is represented in a view-dependent coordinate frame that preserves the layout relationship between the camera view and the scene.

Reprogramming the instance model to a spatial learner and training it in the view-centric space yields a fully feed-forward formulation of interactive scene generator that learns spatial relations directly from instance prior. Via this formulation, training entirely on non-semantic synthetic scenes in which objects are randomly composed without meaningful relations surprisingly yields to strong spatial reasoning ability, surpassing dataset-bounded baselines and robustly generalizes to various layouts.

These results indicate that non-semantic synthetic scenes are sufficient for spatial learning and suggest a promising scaling path for interactive 3D scene understanding and generation. Our contributions are summarized as follows:

- **Model-centric supervision.** We reprogram a pre-trained 3D instance prior to function as a scene-level spatial learner, revealing its transferable spatial knowledge without relying on scene-level annotations.
- **View-centric scene space.** We replace the canonical object space with a view-aligned shared scene representation that preserves geometric and relational cues, enabling a fully feed-forward scene generator.
- **Dataset-independent layout learning.** We show that the reprogrammed instance prior’s strong spatial learning capability from non-semantic, randomly composed synthetic scenes, relaxing annotated data dependency.
- **Strong Generalization.** Despite being trained solely on random layouts, our model surpasses SOTA methods

trained on 3D-FRONT and transfers robustly to diverse unseen layouts.

2. Related Work

Single geometry 3D scene generation. One line of work represents entire scenes as a single global structure guided by text or visual prior. For example, Wonderland [12] predicts 3D Gaussian Splatting in a feed-forward manner from a single image; WonderWorld [29] generates connected scenes from a single view using layered Gaussian surfels. Similarly, WorldExplorer [19]

targets text-driven, 3D-consistent but non-disentangled scenes. These monolithic approaches achieve impressive view consistency and speed, but lack instance accordance, limiting fine-grained editing, instance interaction, and physics reasoning.

Compositional 3D interactive scene generation. Recent pipelines decompose scenes into perception and assembly: instance detection/segmentation and depth provide amodal cues, then objects are retrieved or generated, finally are assembled into a scene. *Gen3DSR* [1] follows a modular divide-and-conquer strategy; *Deep Prior Assembly* [30] integrates frozen priors (e.g., SAM [11], diffusion, Shap-E [10]) with layout fitting; *REPARO* [6] performs compositional asset generation with differentiable 3D layout alignment; *CAST* [27] applies component-aware analysis with SDF-based physics correction. On the text-driven side, graph/LLM planners (e.g., *LayoutGPT* [4], *Holodeck* [25], *GALA3D* [31]) synthesize scene graphs or relational constraints that downstream stages realize with assets and solvers. *Scenethesis* [15] and *SceneWeaver* [26] combines LLM planning, vision guidance, and physics-aware optimization with a plausibility judge. These approaches provide high fidelity and open-ended semantics, but are sensitive to early perception/planning errors, potential retrieval/solver mismatch, and incur per-scene optimization, limiting throughput and scalability.

Learning-based 3D interactive scene generation. Most recent approaches learn spatial layout distributions from curated 3D scene datasets [5], differing mainly in how they instantiate object assets. i) **Layout-first scene synthesis.** model a room as an unordered set of object tokens with attributes such as category, size, pose, which are later instantiated as geometry via retrieval or generation. For instance, *ATISS* [18], *SceneFormer* [22], *DiffuScene* [20], *MiDiffusion* [7], *DeBaRA* [16], and *PhyScene* [24] condition on room type or floor plan, enabling controllable scene completion and synthesis; ii) **End-to-end multi-instance method.** With the advancement of pre-trained image-to-3D object model, recent approaches jointly model multiple objects and their spatial relations, reducing cascade errors and avoiding retrieval/solver loops at test time. *MIDI-3D* [8]

and *SceneGen* [17] model multiple assets and their implicit inter-object relations or instance explicit poses in one feed-forward pass. *PartCrafter* [13] extends compositional latent diffusion transformers to jointly denoise parts/objects into explicit triangle meshes. Both paradigms achieve strong control and coherence but remain constrained by the biases and limited diversity of existing scene datasets, often struggling with rare layouts or complex arrangements such as small objects supported by or occluded behind larger ones.

Our method uses the same input protocol as prior learning-based approaches but differs fundamentally in design. We introduce a feed-forward, view-centric approach that jointly reasons over global scene context and instance generation. This design enables (i) layout generalization beyond dataset biases, capturing richer spatial relations such as small/supporting objects; and (ii) end-to-end inference without retrieval or solver handoffs, avoiding the stage-wise errors and latency of compositional pipelines. Unlike prior methods constrained by curated datasets or optimization-heavy reasoning, our framework could learn spatial knowledge directly from non-semantic synthetic layouts, achieving dataset independence while preserving instance-level editability.

3. Method

3.1. Problem Definition

Given a single image $I_{\text{scene}} \in \mathbb{R}^{H \times W \times 3}$ and its instance masks $\{m_i\}_{i=1}^N$, *I-Scene* generates a set of independently manipulable 3D instances $\mathcal{A} = \{A_i\}_{i=1}^N$, coherently placed in the scene space such that the spatial layout aligns with the input image.

3.2. Overview

Figure 2 presents the overview of our generalizable spatial learner (*I-Scene*). *I-Scene* reprograms an image-to-3D instance foundation model to a spatial learner. We use TRELIS [23] backbone in the experiment. *I-Scene* only modifies the sparse structure transformer. Other stages are kept the same. *I-Scene* has two branches: **spatial guidance branch** and **instance generation branch**. The two branches share the same weight and are trained jointly.

Spatial guidance branch. The spatial guidance branch takes the scene RGB image as input and predicts the scene as a single geometry represented as a sparse set of active voxels. Following TRELIS, the branch outputs

$$f_{\text{scene}} = \{(f_i, p_i)\}_{i=1}^L, \quad (1)$$

where p_i denotes the position of the i -th active voxel, f_i is its corresponding local feature, and L is the number of active voxels. This branch provides two key functions: (i) it produces a global scene layout that guides instance-level generation; and (ii) it establishes a shared scene coordinate

frame (an ‘‘anchor axis’’) that all instances reference. Without this global anchor, instances would be generated independently and the resulting composited scene layout would become incoherent.

Instance generation branch. The instance generation branch takes an instance RGB image I_{inst} as input, conditioned on the spatial guidance latent z_{scene} , and learns a function F to predict voxelized instance features:

$$f_{\text{inst}} = F(I_{\text{inst}}, z_{\text{scene}}), \quad (2)$$

The instance generation not only learns the instance local geometry, but also its pose in the scene. As z_{scene} already provides the scene layout, F just needs to focus on geometry generation and follow the scene layout guidance. This effectively converts the instance generator from implicitly encoding scene priors to explicitly learning spatial layout. This key formulation unlocks generalizable 3D scene generation. In detail, F is achieved by scene-context attention.

3.3. Scene-Context Attention

We not only need to learn F , but also need to preserve the base model’s prior as we do not want z_{scene} to be catastrophically forgotten. So we need to minimize the change to the base model. We present scene-context attention to achieve this goal.

We transform some of the original self-attention layers to scene-context attention (SCA) layers. In the original self-attention layer, let (Q_i, K_i, V_i) be queries/keys/values from instance i and (Q_s, K_s, V_s) be the queries/keys/values from the spatial guidance branch.

$$\tilde{K}_i = [K_i; K_s], \quad \tilde{V}_i = [V_i; V_s], \quad (3)$$

$$\text{SCA}(Q_i, \tilde{K}_i, \tilde{V}_i) = \text{softmax}\left(\frac{Q_i \tilde{K}_i^\top}{\sqrt{d}}\right) \tilde{V}_i, \quad (4)$$

Intuitively, the instance generation is not only based on its own K_i and V_i , but also conditions on K_s and V_s . SCA is a natural modification to the backbone as it does not change the latent distribution, making minimal changes to the prior. An extreme example can demonstrate this property: when the K_i/V_i is the same with the scene K_s/V_s , meaning when the scene and instance input is exact the same, the SCA gives equivalent result of self-attention layers. We show the mathematical proof in the *Appendix*.

3.4. View-Centric (VC) Space

Existing relevant works [8, 17] follow image-to-3D base model and use canonical space for scene representation. We observe using canonical space limits the learning of F and

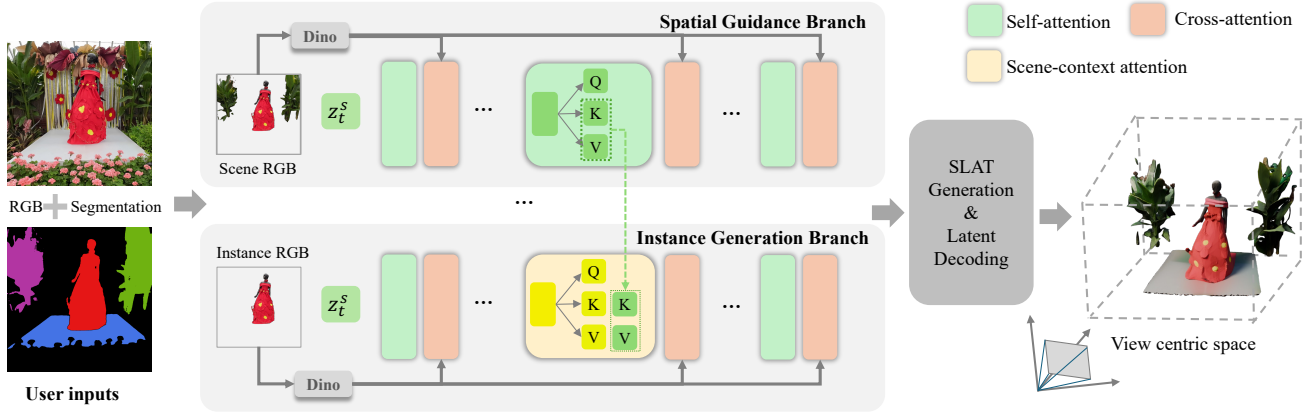


Figure 2. **Overview.** *I-Scene* has two branches: (i) spatial guidance branch takes scene RGB as input and provides spatial anchor for each instance generation. (2) Instance branch takes instance RGB and scene context tokens and output the instance in view centric space.

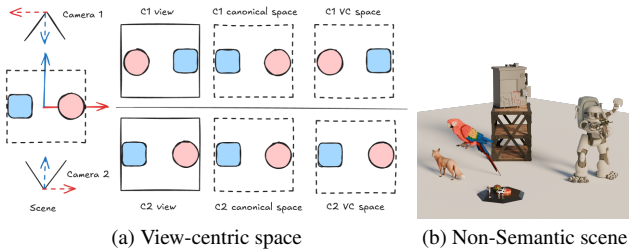


Figure 3. (a). Canonical space scene is view invariant. View centric (VC) space is view-dependent, which encodes strict spatial relationship between the image space and scene space. (b) a non-semantic random 3D scene example. Objects have random poses and are collision-free.

hurts the model generalization ability. As illustrated in Figure 3 (a), given two camera ($C1$ and $C2$) and the scene composed of a blue square and a red circle in the space, the camera views of the scene are different as they are in different location and orientation, but the instance in the scene stay at the same position in the canonical space. So this formulation makes the F ignores the object spatial position in the view image I and only focuses on the local shape of each instance in the image. When training on some indoor dataset like 3D-FRONT, it is not significantly hurting F as there are limited object in the scene and each instance usually has very different shapes. But if the scene has identical objects, e.g. several identical chairs having similar poses, F often put duplicated chairs at the same position. We argue that the object spatial layout in the RGB image is also important and provides strong hint on its 3D layout pose. So we propose view-centric space where the space axis is based on the camera pose. As shown in Figure 3 (a), given the same two camera setting, the spatial layout of the two objects follows the change of the camera pose coherently. When training *I-Scene* in VC space, F achieves much better generalization

results as shown in our ablation study (Table 3).

3.5. Non-Semantic Synthetic 3D Scene

3D-FRONT is a domain specific dataset that only has limited indoor assets. Although with our SCA and VC space, *I-Scene* already achieves the SOTA generalization results (Table 1), we observe the instance quality degrades, implying the model inevitably forgets the instance prior. As the spatial learner F is not directly learning the dataset layout, but learning from the given spatial guidance, we observe that whether the training scene layout has semantic meaning is not very important for *I-Scene*. In the other hand, training on the random scene composed of instances from the whole instance 3D dataset further improve *I-Scene* generalization ability.

Collision-free Random Layout. We generate our synthetic scenes via sampling high-quality 3D instances from a diverse 3D asset dataset (e.g., Objaverse [3]), randomly places them with a collision-free mechanism to reduce severe occlusions, and enforces a common spatial relation such as *right*, *left*, *front*, *back*, and *on the top of*. The scene layout is purely non-semantic meaningful composition of instance; only geometric and basic physical plausibility constraints are applied. By training on this dataset, *I-Scene* learns general spatial reasoning while remaining agnostic to category semantics. We provide our random layout generation details in appendix.

3.6. Training

The training target is conditioned rectified flow methods:

$$\mathcal{L}_{CFM}(\theta) = \mathbb{E}_{t, x_0, \epsilon} \|v_\theta(x, t) - (\epsilon - x_0)\|_2^2, \quad (5)$$

where v_θ is the sparse structure neural network, $x(t) = (1 - t)x_0 + t\epsilon$, and ϵ is the noise at time step t .

4. Experiment

4.1. Experiment Setting

Baseline. We compare the representative interactive 3D scene generation methods including MIDI [8], Scene-Gen [17], PartCrafter [13], and Gen3DSR [1].

For all baselines, we use the same scene RGB image and instance masks as inputs, except PartCrafter, which does not support mask control; for PartCrafter we provide the scene RGB plus the target instance count. Because PartCrafter lacks texture rendering, we evaluate it only on scene-level geometry and layout quality. For visual quality comparisons, we texture MIDI’s generated scenes using MV-Adapter [9].

Metric. We evaluate scenes based on geometry quality and layout accuracy. For geometry quality, we convert the generated assets to point clouds and rigidly align the prediction to the ground truth using customized robust ICP (details in *appendix*).

After alignment, we then report Chamfer Distance (CD) and F-Score (threshold $\tau=0.1$) at two levels: (i) *scene level* on the union of all points, and (ii) *object level* by computing the metrics per matched instance and averaging.

To evaluate scene layout, we compute matched volumetric IoU between the axis-aligned bounding boxes (AABBs) of predicted and ground-truth scenes. This metric captures the overall objects size, position, and relative placement.

We also report the average inference time per instance.

Evaluation Dataset. We evaluate all methods on **synthetic** data and **real-world/stylized** scenes. i) *Synthetic (in-domain)*. Following MIDI, we adopt the 3D-FRONT split and use the same test scenes, filtering out renders with fully occluded instance masks; this yields ~ 860 test scenes. ii) *Synthetic (out-of-domain)*. To assess generalization to novel layouts and object sets, we additionally evaluate on scenes from BlendSwap [2] and Scenethesis [15], which yield 26 test scenes including small on large relations and outdoor settings. iii) *Real-world /stylized*. For in-the-wild evaluation without ground truth, we test on images from DL3DV-140 [14], Gen3DSR [1], ScanNet++ [28], and stylized scenes. Then, we report qualitative comparisons.

4.2. Quantitative Results

Table 1 reports quantitative comparisons on synthetic datasets, including 3D-FRONT [5], BlendSwap [2], and Scenethesis [15]. 3D-FRONT dataset only contains bedroom/living room scenarios, while Blendswap and Scenethesis contain more diverse layout. Our method, *I-Scene*, achieves the best performance among the state-of-the-art methods across all evaluated metrics without incurring much time consumption.

Geometry quality. *Object-level.* On 3D-FRONT test scenes (ID), our method attains the *lowest* object-level CD

and the *highest* F-score compared with MIDI [8], Scene-Gen [17], PartCrafter [13], and Gen3DSR [1], indicating higher-fidelity per-object geometry. Crucially, on out-of-domain (OOD) benchmarks (BlendSwap, Scenethesis), our object-level scores remain *comparable to ID* and still exceed all baselines by a clear margin, evidencing robust generalization. *Scene-level.* Across both ID and OOD settings, our method also achieves *lowest* scene-level CD and *highest* F-score than the baselines, reflecting more accurate and more complete whole-scene geometry. We attribute these gains to: i) **reprogrammed a pre-trained instance prior**. A pre-trained instance generator supplies strong single-object shape priors, which is an advantage over methods rely primarily on reconstruction from limited data such as Gen3DSR; ii) **model-centric supervision with shared, view-centric scene context**. Per-instance generation conditioned on shared, view-centric scene tokens keeps shapes near canonical while aligning pose and contact, reducing fused-mesh artifacts and “shape bending” common in scene dataset-supervised methods such as MIDI, Scene-Gen, PartCrafter. Unlike all baselines, which degrade substantially on OOD scenes, our object- and scene-level metrics on BlendSwap and Scenethesis remain close to our ID scene performance, underscoring strong generalization.

Layout accuracy. Our method attains the highest *Volumetric IoU* across all baselines, indicating more accurate object placement in position, scale, and orientation and global scene geometry consistency. Gains are largest on *BlendSwap/Scenethesis*.

Our results suggest stronger modeling of support and proximity for various layout. The metric result also confirm the advancement of *I-Scene* from scene and instance geometry quality. The instance semantic and spatial relation disentangled formulation improves scene-level fidelity without additional scene annotations.

Efficiency. We measure end-to-end per instance inference time on a single H100 GPU for all approaches. Our method completes a instance in 15.51s, although slower than PartCrafter (7.2 s) while delivering higher geometry and layout quality, and faster than the other baselines in our study. For fairness, MIDI inference time includes per instance texture rendering. We attribute our latency to a feed-forward design leveraging the pre-trained instance prior, which avoids retrieval or iterative layout optimization.

4.3. Qualitative results

We qualitatively compare our approach with MIDI, Scene-Gen, PartCrafter, and Gen3DSR in two settings: (i) **synthetic scenes** and (ii) **real-world and stylized inputs**.

All methods receive the same single input image.

Synthetic scenes Figure 4 contrasts our results on 3D-FRONT-style scenes and more complicated layouts from BlendSwap and Scenethesis. **Instance quality.** Our

Table 1. Comparison on evaluation datasets. CD: Chamfer Distance; F-Score threshold $\tau=0.1$. S = scene-level; O = object-level; IoU-B = volumetric IoU of scene bounding boxes. Best numbers are in **bold**. PartCrafter is only compared on scene-level performance.

Method	3D-FRONT					BlendSwap & Scenethesis					Runtime↓
	CD-S↓	F-Score-S↑	CD-O↓	F-Score-O↑	IoU-B↑	CD-S↓	F-Score-S↑	CD-O↓	F-Score-O↑	IoU-B↑	
Gen3DSR	0.2587	42.31	0.0697	57.22	0.4838	0.1429	45.43	0.0722	53.45	0.4736	179.0 s
PartCrafter	0.0586	81.03	-	-	0.7626	0.0609	66.56	-	-	0.5819	7.2 s
SceneGen	0.1432	54.70	0.0353	77.95	0.5295	0.1161	49.94	0.0852	65.66	0.4669	26.0 s
MIDI	0.0175	90.08	0.0877	70.10	0.8596	0.0212	83.13	0.1884	50.84	0.7412	42.5 s
Ours	0.0148	93.50	0.0207	84.28	0.8762	0.0059	94.26	0.0503	72.39	0.8568	15.51 s

Table 2. Comparison on **3D-FRONT** and **BlendSwap & Scenethesis**. CD: Chamfer Distance; F-Score threshold $\tau=0.1$. S = scene-level, O = object-level; IoU-B = volumetric IoU of scene bounding boxes. Best numbers are **bold**.

Training dataset	3D-FRONT					BlendSwap & Scenethesis				
	CD-S↓	F-Score-S↑	CD-O↓	F-Score-O↑	IoU-B↑	CD-S↓	F-Score-S↑	CD-O↓	F-Score-O↑	IoU-B↑
3D-FT (25K)	0.0137	93.77	0.0278	81.34	0.8792	0.0118	90.79	0.0585	68.87	0.8222
Rand-15K	0.0496	79.96	0.0932	55.01	0.7729	0.0081	92.67	0.0698	67.36	0.8445
Rand-25K	0.0406	81.39	0.0402	74.76	0.7783	0.0075	93.60	0.0580	70.18	0.8471
3D-FT+Rand-15K	0.0148	93.50	0.0207	84.28	0.8762	0.0059	94.26	0.0503	72.39	0.8568

method produces *clean, well-separated* instance meshes with sharp thin parts (e.g., shelf, sofa, umbrella in the figure) and minimal artifacts, aligning with the lower object-level CD and higher F-score in Sec. 4.2. Baseline methods such as MIDI and SceneGen often exhibit *duplicate placements, uncleaned mesh*, or *over-smoothed geometries* that blur instance boundaries. **Spatial relations.** Our scenes preserve *support* and *proximity* (e.g., small-on-large relations such as TV/ flower on tables), maintain correct *depth ordering* for partially *behind/occluded* items, and avoid *floating* or *colliding* objects, which is common in baselines. This is consistent with our higher Volumetric IoU and scene-level F-score. **Robustness on various layouts.** Gains are most visible on BlendSwap and Scenethesis testing scenes, which include multi-scale clutter, small-on-large configurations, and outdoor layouts that are under-represented in curated indoor datasets.

Real-world and stylized scenes We further evaluate on in-the-wild images from DL3DV-140, Gen3DSR, and ScanNet++ and on stylized/cartoon inputs as shown in Figure 5. Across these distributions, baselines are less robust to strong style shifts and complex layouts, frequently showing *misaligned instances*, *surface bleed* between nearby assets, and *implausible supports* such as frequently collided objects. In contrast, our method maintains **consistent scale and uprightness, clear separation between instances, and plausible contacts** across indoor, outdoor, and stylized scenes.

Comparison with baselines. Existing feed-forward or retrieval/assembly pipelines tend to either sacrifice per-object fidelity or lose global coherence when generalize to

novel layouts: duplicate objects, merged/entangled assets, collided and floating placements are common failure modes. Our results exhibit both *higher per-instance fidelity* and *more coherent spatial relations*, which we attribute to i) **model-centric supervision** from a reprogrammed pre-trained instance prior (preserving object fidelity) and ii) **view-centric shared scene context** that stabilizes relative pose, depth ordering, and support for each instance from a shared space during generation. The Appendix includes additional synthetic/real/stylized examples, multi-view renderings for each scene, and videos for large scenes with complex layouts.

4.4. Non-semantic random scene experiment

In this section, we want to answer the **question**: *do non-semantic, randomly composed scenes provide meaningful spatial supervision?*

Setup. To answer the question, we conduct the experiment that train *I-Scene* on four datasets: i) **3D-FT**: 25K 3D-FRONT scenes including bedroom/living-room with dedicated scene annotations. ii) **Rand-15K**: 15K non-semantic scenes by randomly composing instances. It is generated by our synthetic data generation system. iii) **Rand-25k**: same as Rand-15K but scaled to 25K scenes. iv) **3D-FT+Rand-15K**: a mixture of 3D-FT and Rand-15K. **Evaluation.** The 3D-FRONT test set is treated as *in-distribution* for model trained on 3D-FT. BlendSwap and Scenethesis contain more diverse layouts and are used as *out-of-distribution (OOD)* benchmarks.

Result. Table 2 presents the experiment results. We observe that training solely on 3D-FRONT (3D-FT) yields



Figure 4. Qualitative comparison with all baselines on synthetic scenes. We might slightly rotate the view to better illustrate the error patterns. More details can be found in *Appendix*.

Table 3. Ablation on *I-Scene*’s components. SCA: scene context attention, VC: view centric, NS: non-semantic scenes.

Examine component			3D-FRONT					BlendSwap & Scenethesis				
SCA	VC	NS	CD-S↓	F-Score-S↑	CD-O↓	F-Score-O↑	IoU-S↑	CD-S↓	F-Score-S↑	CD-O↓	F-Score-O↑	IoU-S↑
✓	✗	✗	0.0163	93.69	0.0286	80.12	0.8598	0.0351	79.12	0.0829	63.16	0.7557
✓	✓	✗	0.0137	93.77	0.0278	81.34	0.8792	0.0118	90.79	0.0585	68.87	0.8222
✓	✓	✓	0.0148	93.50	0.0207	84.28	0.8762	0.0059	94.26	0.0503	72.39	0.8568

the stronger in-distribution layout (lowest CD-S, highest IoU-B) compared to purely trained on non-semantic scenes, but generalizes poorly to BlendSwap/Scenethesis (OOD). Interestingly, purely non-semantic randomized training (Rand-15k/25k) captures transferable spatial regularities and surpasses 3D-FT on BlendSwap/Scenethesis scene-level metrics (CD-S↓, F-S↑, IoU-B↑), with performance improving as we scale from 15k to 25k scenes. The combined regimen (3D-FT+Rand-15k) preserves near-optimal in-domain layout while further improving object geometry (lower CD-O, higher F-O) and achiev-

ing the best OOD results across all metrics.

These findings indicate that i) *I-Scene* is able to learn spatial knowledge from *non-semantic* scenes. In particular, instead of the high-level scene semantics, **geometric cue alone provides a strong training signal** for spatial learning and reasoning. ii) Curated scene annotations remain useful for *in-distribution calibration*, *synergizing training* with non-semantic scenes to yield the best overall performance. and iii) Non-semantic spatial relations are a valuable supervision source; **scaling non-semantic data provides richer spatial coverage that the model can exploit**.

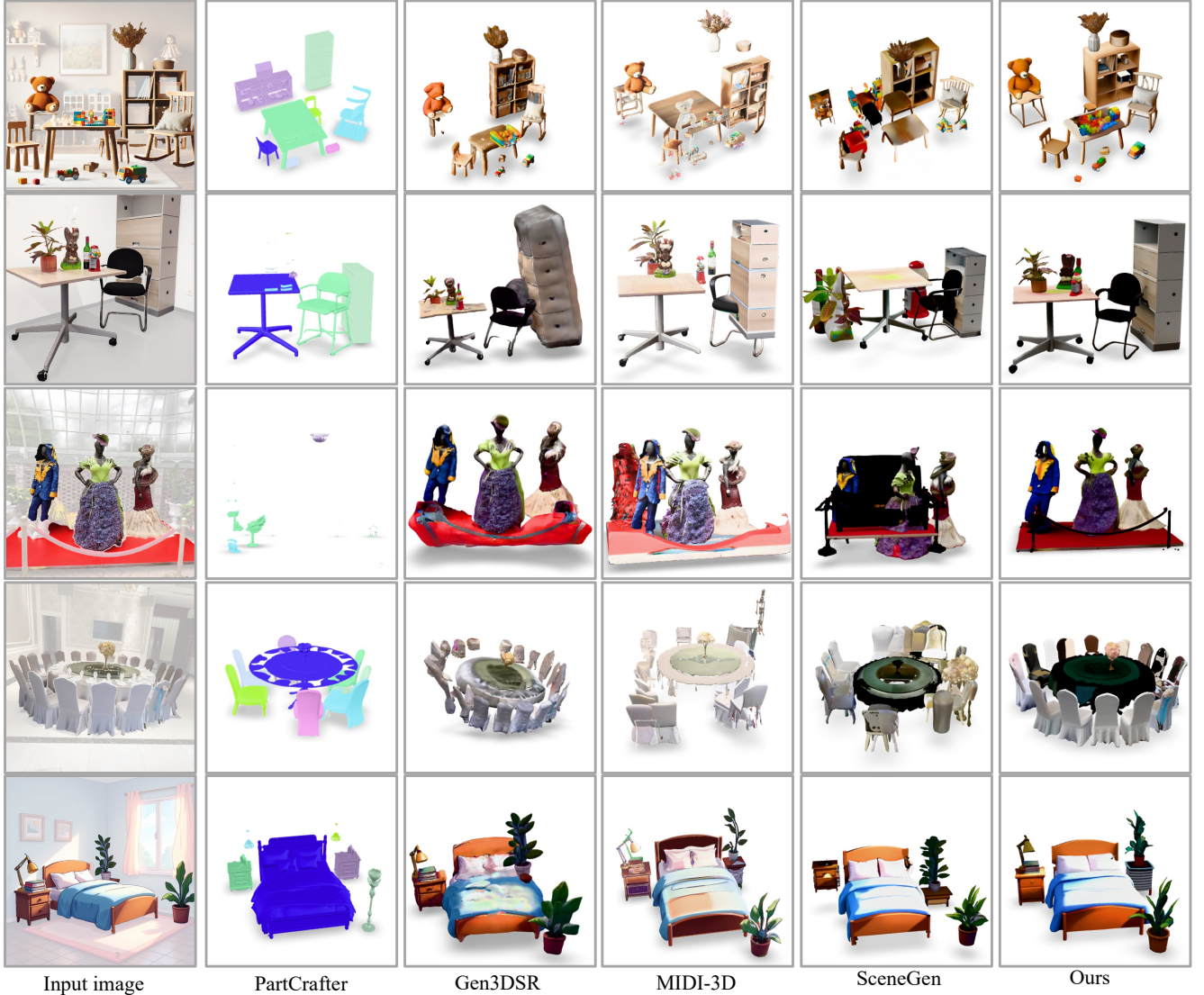


Figure 5. Qualitative comparison with scenes in-the-wild. We compare the generalization ability of different methods in different style and various spatial relations. To better illustrate the error pattern, we might slightly rotate the view.

4.5. Ablation studies

We evaluate the contribution of the main design choices in *I-Scene* on 3D-FRONT, BlendSwap, and Scenethesis. We study three components: (i) **Scene-context attention(SCA)**: shared scene-level tokens that contain spatial cues; (ii) **View-centric(VC)**: the view-aligned space; (iii) **Non-semantic meaningful scenes (NS)**: randomized compositions from the Objaverse instances.

We start from the full model ($SCA + VC + NS$) and remove one component at a time. As summarized in Table 3, we observe that **every component matters**. Removing any of SCA, VC, NS consistently degrades geometry ($CD\uparrow$, $F\text{-score}\downarrow$) and layout accuracy ($IoU\downarrow$) on all evalua-

tion datasets, confirming their complementary roles in *I-Scene* for generalize to novel layout. **VC is critical for layout coherence**. Without view-centric encoding, the model tends to over-fit on 3D-FRONT dataset and has poor generalized results on Blendswap and Scenethesis. It also misaligns scene context across objects, yielding duplicated or “blended” instances and contact violations; this manifests as the largest IoU drop and a notable decline in scene-level F-score. **NS improves instance generalization**.

Adding NS yields substantial gains in F-score at the instance level and increment in spatial-relation (IoU), reflecting better surface completeness and fewer near-surface errors for new scenes and inter-object placement is driven chiefly by the view-centric shared scene context. We pro-

vide qualitative results for the ablation study in *appendix*. Overall, these results demonstrate that view-centric scene context (VC+SC) is essential for coherent layouts and clean instance boundaries, while training on non-semantic scene (NS) supplies the instance diversity needed to generalize beyond distributions.

5. Conclusion

Contribution. We reprogram a pre-trained 3D *instance* generator as a scene-level spatial learner. We define a *view-centric* scene space and distill spatial cues into shared *scene tokens* that condition instance denoising, yielding a fully *feed-forward* formulation for interactive scene generation. This formulation replaces dataset-bounded layout supervision with model’s own spatial prior, removing reliance on curated scene annotations and enabling learning spatial relations from *non-semantic* meaningful scenes. Our experiments indicate non semantic meaningful synthetic data improve geometry, layout, and generalization, pointing toward a foundation model for interactive 3D scene generation.

Limitations and future work. Our method performs relatively poorly on tiny-resolution inputs and in heavily occluded single-view case (see *Appendix*). Future work: 1) improve model robustness with heavy occlusion augmentations, and to explore optional multi-view conditioning; 2) Further investigate the scaling law of non-semantic random scene to further handle challenging in-the-wild layouts.

I-Scene: 3D Instance Models are Implicit Generalizable Spatial Learners

Supplementary Material

6. Overview

To better illustrate our method, the supplementary material is organized into two main parts: **Method** and **Experiments**. In addition, we provide an **HTML** page for improved qualitative visualization and comparison.

Method.

- **Scene-context attention.** We provide a mathematical derivation showing that when the scene and instance inputs are identical, the proposed scene-context attention (SCA) is equivalent to a standard self-attention layer.
- **Collision-free random layout.** We describe the details of our collision-free random layout generation procedure.

Experiment setting.

- Model implementation details.
- Training datasets.
- Metrics. We provide the full specification of our customized robust ICP metric and related details.

Qualitative results.

- Qualitative comparison with all baselines on synthetic scenes. We either (i) show interactive 3D scene comparisons on the web page, or (ii) include two representative rendered views per scene for each method.
- Qualitative comparison with all baselines on real-world and stylized images, following the same visualization protocol as above.
- Additional qualitative results for the **ablation** study.
- **Failure cases.** We report the failure cases when instance mask is small. The figure including the input image, the predicted scene, and the predicted low-quality instance examples.

7. Method

scene-context attention. In this section, we show the mathematic proof that when the K_i/V_i is the same with the scene K_s/V_s , meaning when the scene and instance input is exact the same, the SCA gives equivalent result of self-attention layers.

Let $Q_i \in \mathbb{R}^{t \times d}$ be the (row-stacked) instance queries, $K_i, K_s \in \mathbb{R}^{n \times d}$ the keys, and $V_i, V_s \in \mathbb{R}^{n \times d_v}$ the values. We concatenate along the token dimension,

$$\tilde{K}_i = [K_i; K_s] \in \mathbb{R}^{2n \times d}, \quad \tilde{V}_i = [V_i; V_s] \in \mathbb{R}^{2n \times d_v},$$

and define scene-context attention (SCA) by

$$\text{SCA}(Q_i, \tilde{K}_i, \tilde{V}_i) = \text{softmax}\left(\frac{Q_i \tilde{K}_i^\top}{\sqrt{d}}\right) \tilde{V}_i,$$

where $\text{softmax}(\cdot)$ is applied *row-wise* across the key dimension. We show that when the scene and instance inputs coincide, i.e., $K_i = K_s$ and $V_i = V_s$, SCA reduces exactly to standard self-attention:

$$\text{SCA}(Q_i, \tilde{K}_i, \tilde{V}_i) = \text{softmax}\left(\frac{Q_i K_s^\top}{\sqrt{d}}\right) V_s.$$

Proposition. If $K_i = K_s$ and $V_i = V_s$, then

$$\text{SCA}(Q_i, [K_i; K_s], [V_i; V_s]) = \text{softmax}\left(\frac{Q_i K_s^\top}{\sqrt{d}}\right) V_s.$$

Proof. Under $K_i = K_s$ and $V_i = V_s$, write $K := K_s$ and $V := V_s$. Then $\tilde{K}_i = [K; K]$ and $\tilde{V}_i = [V; V]$. Let

$$Z := \frac{Q_i K^\top}{\sqrt{d}} \in \mathbb{R}^{t \times n}.$$

By block structure,

$$\frac{Q_i \tilde{K}_i^\top}{\sqrt{d}} = \frac{Q_i [K; K]^\top}{\sqrt{d}} = [Z \quad Z] \in \mathbb{R}^{t \times 2n}.$$

Consider any row $z \in \mathbb{R}^n$ of Z . The row-wise softmax over the concatenation $[z, z] \in \mathbb{R}^{2n}$ yields

$$\text{softmax}([z, z]) = \left[\frac{1}{2} \text{softmax}(z) \quad \frac{1}{2} \text{softmax}(z) \right],$$

because for each coordinate j , with $s := \sum_{\ell=1}^n e^{z_\ell}$ we have

$$\frac{e^{z_j}}{\sum_{\ell=1}^n e^{z_\ell} + \sum_{\ell=1}^n e^{z_\ell}} = \frac{e^{z_j}}{2s} = \frac{1}{2} \text{softmax}(z)_j.$$

Applying this row-wise to $[Z, Z]$ gives

$$\text{softmax}([Z, Z]) = \left[\frac{1}{2} S \quad \frac{1}{2} S \right], \quad \text{where}$$

$$S := \text{softmax}(Z) \in \mathbb{R}^{t \times n}.$$

Therefore,

$$\begin{aligned} \text{softmax}([Z, Z]) \tilde{V}_i &= \left[\frac{1}{2} S \quad \frac{1}{2} S \right] [V; V] \\ &= \frac{1}{2} S V + \frac{1}{2} S V \\ &= S V \\ &= \text{softmax}\left(\frac{Q_i K^\top}{\sqrt{d}}\right) V. \end{aligned} \tag{6}$$

This is precisely the output of a standard self-attention layer evaluated on (Q_i, K, V) . ■

Collision-free Random Layout. When we randomly create a layout, we first randomly sample N instances from the instance object dataset (e.g. Objaverse). Then we generate collision-free layouts in a Poisson noise pattern by treating each object i as a 2D disc on the ground with radius $r_i = s_i \hat{r}_i$, where \hat{r}_i is computed from the mesh x/z extents and s_i is the sampled scale. Centers are sampled with a variable-radius Poisson-disk routine that places larger radius first. We define a global clearance gap $= \bar{r} \cdot s$, where \bar{r} is the mean of r_i and s is a randomly sampled scaling factor that controls the layout density. A candidate center \mathbf{x}_i is accepted only if $\|\mathbf{x}_i - \mathbf{x}_j\|_2 \geq r_i + r_j + \text{gap}$ for all placed j . We accelerate checks with a uniform grid of cell size $(\min_i r_i + \text{gap})/\sqrt{2}$, retry up to a fixed budget, and expand the sampling region by 10% if needed. When a table is present, it is placed first and included in the same exclusion process. For the stacked object, we slice the table mesh just below its top to extract the top polygon, use its centroid as the anchor, and choose a scale that fits inside based on the distance to the nearest edge, then place the stacked object on the table.

8. Experiment

Model implementation. All experiments are conducted on a cluster with 8 NVIDIA H100 GPUs. We train *I-Scene* for 130K steps using the AdamW optimizer with a learning rate of $5e^{-5}$ and a batch size of 8 per GPU. During inference, we adopt 25 sampling steps with the classifier-free guidance set to $\omega = 3.0$ for both the sparse structure generation and structured latents generation.

Training dataset The 3D-FRONT training dataset is the same as MIDI processed 3D-FRONT dataset, where there are roughly 24K different scenes. Using the random layout generation algorithm discussed above, randomly generate 15K and 25K scenes. Each scene has minimum 2 object and maximum 12 objects.

For each scene, we use Blender to render 150 views that evenly distributed from all directions looking at the scene center. Then we transform each instance into view centric space, voxelize and encode each instance geometry using TRELLIS sparse structure encoder as ground truth. Note, in some view some object is fully occluded and not visible, we discard this render view to avoid the model memorize and hallucinate invisible objects.

Robust ICP. Previous work MIDI [8] uses ICP for alignment before calculating the metrics. We notice this ICP is not robust and leads to many bad alignment, making the metric calculation not reliable. Instead, we propose a robust ICP to make the metric results more reliable.

The main reason ICP is not robust is it is very easy to

get stuck into local minimum. To handle this challenge, we used several ways to escape local minimum.

Initial transform search. We perform a yaw-sweep global initialization about a designated up axis ($a \in \{x, y, z\}$). For a candidate set of yaw angles (default $\{0, 45, 90, 135, 180, 225, 270, 315\}$ degrees), we rotate the source downsampled point cloud about a , and pre-score each angle using a trimmed symmetric Chamfer distance with trim ratio $\tau=0.2$ on up to 2000 sampled points per cloud. We keep the top three yaw candidates by this pre-score and run a short seed ICP on the downsampled clouds for each candidate using a point-to-point estimator (optionally with isotropic scale if enabled). We select the initialization T_0 that minimizes $\text{rmse} + \lambda(1 - \text{fitness})$ with λ set to the voxel size ($\lambda=v$).

Coarse-to-fine. *Shared normalization.* For numerical stability and consistency across stages, we apply the same uniform normalization to source and target: let c be the mid-point of the axis-aligned bounding box over both clouds and σ the maximum side length. We work in normalized coordinates $x' = (x - c)/\sigma$ for the remainder of the registration.

Downsampling and normals. We voxel downsample both normalized clouds with voxel size $v = 0.03$ (relative to the normalized extent) for the coarse stage, and estimate normals on both downsampled and full-resolution clouds when available.

Estimators. The coarse stage uses a point-to-point objective; if isotropic scale is enabled and supported, we estimate a global uniform scale jointly with the rigid motion. The fine stage uses point-to-plane with a Tukey robust loss (scale $k = 1.5v$); if normals or robust losses are unavailable, we fall back to point-to-point.

Iteration budgets and thresholds. We split the budget evenly with safeguards: $T_{\text{coarse}} = \max(10, \lfloor 0.5T \rfloor)$ and $T_{\text{fine}} = \max(10, T - T_{\text{coarse}})$. Distance thresholds are $2.5v$ (coarse) and v for point-to-plane fine refinement (or $1.5v$ if point-to-point is used).

Execution. Coarse ICP is run on the downsampled pair from T_0 , yielding T_{coarse}^* . If isotropic scale was estimated, we pre-apply T_{coarse}^* to the full-resolution source and run fine ICP from identity, then compose the results; otherwise, we run fine ICP on the full-resolution pair initialized with T_{coarse}^* .

Pose projection and validation. We project the 3×3 rotation block to the nearest element of $\text{SO}(3)$ via SVD. If reflections are disallowed, we enforce a positive determinant. We then perform sanity checks on the transform in normalized space (finite entries, reasonable determinant when rigid, translation magnitude not excessive). On detection

of anomalies we fall back to the coarse solution or identity, whichever is valid.

Practical notes. As different methods generate in different space with various scale, this introduces a subtle bias. Even if we align the space by min/max values, the scene size potentially still affects the results. For example, rotating an extreme long scene a little bit potentially has different scene scale after normalization. So we apply the robust ICP alignment in this way, say we have two space: (i). min/max normalize space: just scale the scene space by the default output range, e.g. TRELLIS outputs into $[-0.5, 0.5]$, then we just scale the scene isotropically by 2; (ii). AABB re-centered normlize: we move the scene into zero center and then normalize AABB min/max into $[-1.0, 1.0]$. We apply robust ICP and obtain $transform_1$ and $transform_2$. We then pick the best metric results from the two transformations.

9. Qualitative results.

We present the qualitative results for the following items:

- [Figure 6](#) and [Figure 7](#) present multi-view qualitative comparison between *I-Scene* and all baselines using real-world/stylized images as input.
- [Figure 8](#) presents multi-view qualitative comparison between *I-Scene* and all baselines using synthetic scene images as input.
- The visualization of ablation study can be found in [Figure 9](#), where adding each component (SCA, VC, and NS) in *I-Scene* would significantly improve the layout coherent and instance quality.
- We also present the failure cases in [Figure 10](#). As shown in the figure, instance quality is bad when the input instance mask is small in the image.

References

- [1] Andreea Ardelean, Mert Özer, and Bernhard Egger. Gen3dsr: Generalizable 3d scene reconstruction via divide and conquer from a single view. *arXiv preprint arXiv:2404.03421*, 2024. [2](#), [5](#), [6](#), [7](#)
- [2] Dejan Azinović, Ricardo Martin-Brualla, Dan B Goldman, Matthias Nießner, and Justus Thies. Neural rgb-d surface reconstruction. In *Proceedings of the IEEE/CVF Conference on Computer Vision and Pattern Recognition*, pages 6290–6301, 2022. [5](#)
- [3] Matt Deitke, Dustin Schwenk, Jordi Salvador, Luca Weihs, Oscar Michel, Eli VanderBilt, Ludwig Schmidt, Kiana Ehsani, Aniruddha Kembhavi, and Ali Farhadi. Objaverse: A universe of annotated 3d objects. In *Proceedings of the IEEE/CVF conference on computer vision and pattern recognition*, pages 13142–13153, 2023. [4](#)
- [4] Weixi Feng, Wanrong Zhu, Tsu-jui Fu, Varun Jampani, Arjun Akula, Xuehai He, Sugato Basu, Xin Eric Wang, and William Yang Wang. Layoutgpt: Compositional visual planning and generation with large language models. *Advances in Neural Information Processing Systems*, 36:18225–18250, 2023. [2](#)
- [5] Huan Fu, Bowen Cai, Lin Gao, Ling-Xiao Zhang, Jiaming Wang, Cao Li, Qixun Zeng, Chengyue Sun, Rongfei Jia, Binqiang Zhao, et al. 3d-front: 3d furnished rooms with layouts and semantics. In *Proceedings of the IEEE/CVF International Conference on Computer Vision*, pages 10933–10942, 2021. [1](#), [2](#), [5](#)
- [6] Haonan Han, Rui Yang, Huan Liao, Jiankai Xing, Zunnan Xu, Xiaoming Yu, Junwei Zha, Xiu Li, and Wanhua Li. Reparo: Compositional 3d assets generation with differentiable 3d layout alignment. *arXiv preprint arXiv:2405.18525*, 2024. [2](#)
- [7] Siyi Hu, Diego Martin Arroyo, Stephanie Debats, Fabian Manhardt, Luca Carlone, and Federico Tombari. Mixed diffusion for 3d indoor scene synthesis. *arXiv preprint arXiv:2405.21066*, 2024. [2](#)
- [8] Zehuan Huang, Yuan-Chen Guo, Xingqiao An, Yunhan Yang, Yangguang Li, Zi-Xin Zou, Ding Liang, Xihui Liu, Yan-Pei Cao, and Lu Sheng. Midi: Multi-instance diffusion for single image to 3d scene generation. In *Proceedings of the Computer Vision and Pattern Recognition Conference*, pages 23646–23657, 2025. [1](#), [2](#), [3](#), [5](#), [6](#), [7](#)
- [9] Zehuan Huang, Yuan-Chen Guo, Haoran Wang, Ran Yi, Lizhuang Ma, Yan-Pei Cao, and Lu Sheng. Mv-adapt: Multi-view consistent image generation made easy. In *Proceedings of the IEEE/CVF International Conference on Computer Vision*, pages 16377–16387, 2025. [5](#)
- [10] Heewoo Jun and Alex Nichol. Shap-e: Generating conditional 3d implicit functions. *arXiv preprint arXiv:2305.02463*, 2023. [2](#)
- [11] Alexander Kirillov, Eric Mintun, Nikhila Ravi, Hanzi Mao, Chloe Rolland, Laura Gustafson, Tete Xiao, Spencer Whitehead, Alexander C Berg, Wan-Yen Lo, et al. Segment anything. In *Proceedings of the IEEE/CVF international conference on computer vision*, pages 4015–4026, 2023. [2](#)
- [12] Hanwen Liang, Junli Cao, Vidit Goel, Guocheng Qian, Sergei Korolev, Demetri Terzopoulos, Konstantinos N Plataniotis, Sergey Tulyakov, and Jian Ren. Wonderland: Navigating 3d scenes from a single image. In *Proceedings of the Computer Vision and Pattern Recognition Conference*, pages 798–810, 2025. [2](#)
- [13] Yuchen Lin, Chenguo Lin, Panwang Pan, Honglei Yan, Yiqiang Feng, Yadong Mu, and Katerina Fragkiadaki. Partcrafter: Structured 3d mesh generation via compositional latent diffusion transformers. *arXiv preprint arXiv:2506.05573*, 2025. [3](#), [5](#), [6](#), [7](#)
- [14] Lu Ling, Yichen Sheng, Zhi Tu, Wentian Zhao, Cheng Xin, Kun Wan, Lantao Yu, Qianyu Guo, Zixun Yu, Yawen Lu, et al. D3dv-10k: A large-scale scene dataset for deep learning-based 3d vision. In *Proceedings of the IEEE/CVF Conference on Computer Vision and Pattern Recognition*, pages 22160–22169, 2024. [5](#)
- [15] Lu Ling, Chen-Hsuan Lin, Tsung-Yi Lin, Yifan Ding, Yu Zeng, Yichen Sheng, Yunhao Ge, Ming-Yu Liu, Aniket Bera,

- and Zhaoshuo Li. Scenethesis: A language and vision agentic framework for 3d scene generation. *arXiv preprint arXiv:2505.02836*, 2025. 2, 5
- [16] Léopold Maillard, Nicolas Sereyjol-Garros, Tom Durand, and Maks Ovsjanikov. Debara: Denoising-based 3d room arrangement generation. *Advances in Neural Information Processing Systems*, 37:109202–109232, 2024. 2
- [17] Yanxu Meng, Haoning Wu, Ya Zhang, and Weidi Xie. Scenegen: Single-image 3d scene generation in one feedforward pass. *arXiv preprint arXiv:2508.15769*, 2025. 1, 3, 5, 6, 7
- [18] Despoina Paschalidou, Amlan Kar, Maria Shugrina, Karsten Kreis, Andreas Geiger, and Sanja Fidler. Atiss: Autoregressive transformers for indoor scene synthesis. *Advances in Neural Information Processing Systems*, 34:12013–12026, 2021. 2
- [19] Manuel-Andreas Schneider, Lukas Höllein, and Matthias Nießner. Worldexplorer: Towards generating fully navigable 3d scenes. In *SIGGRAPH Asia 2025 Conference Papers*, pages 1–11, 2025. 2
- [20] Jiapeng Tang, Yinyu Nie, Lev Markhasin, Angela Dai, Justus Thies, and Matthias Nießner. Diffuscene: Denoising diffusion models for generative indoor scene synthesis. In *Proceedings of the IEEE/CVF conference on computer vision and pattern recognition*, pages 20507–20518, 2024. 1, 2
- [21] Dmitry Tochilkin, David Pankratz, Zexiang Liu, Zixuan Huang, Adam Letts, Yangguang Li, Ding Liang, Christian Laforte, Varun Jampani, and Yan-Pei Cao. Triposr: Fast 3d object reconstruction from a single image. *arXiv preprint arXiv:2403.02151*, 2024. 1
- [22] Xinpeng Wang, Chandan Yeshwanth, and Matthias Nießner. Sceneformer: Indoor scene generation with transformers. In *2021 International Conference on 3D Vision (3DV)*, pages 106–115. IEEE, 2021. 2
- [23] Jianfeng Xiang, Zelong Lv, Sicheng Xu, Yu Deng, Ruicheng Wang, Bowen Zhang, Dong Chen, Xin Tong, and Jiaolong Yang. Structured 3d latents for scalable and versatile 3d generation. In *Proceedings of the Computer Vision and Pattern Recognition Conference*, pages 21469–21480, 2025. 1, 3
- [24] Yandan Yang, Baoxiong Jia, Peiyuan Zhi, and Siyuan Huang. Physcene: Physically interactable 3d scene synthesis for embodied ai. In *Proceedings of the IEEE/CVF Conference on Computer Vision and Pattern Recognition*, pages 16262–16272, 2024. 1, 2
- [25] Yue Yang, Fan-Yun Sun, Luca Weihs, Eli VanderBilt, Alvaro Herrasti, Winson Han, Jiajun Wu, Nick Haber, Ranjay Krishna, Lingjie Liu, et al. Holodeck: Language guided generation of 3d embodied ai environments. In *Proceedings of the IEEE/CVF Conference on Computer Vision and Pattern Recognition*, pages 16227–16237, 2024. 2
- [26] Yandan Yang, Baoxiong Jia, Shujie Zhang, and Siyuan Huang. Sceneweaver: All-in-one 3d scene synthesis with an extensible and self-reflective agent. *arXiv preprint arXiv:2509.20414*, 2025. 2
- [27] Kaixin Yao, Longwen Zhang, Xinhao Yan, Yan Zeng, Qixuan Zhang, Lan Xu, Wei Yang, Jiayuan Gu, and Jingyi Yu. Cast: Component-aligned 3d scene reconstruction from an rgb image. *ACM Transactions on Graphics (TOG)*, 44(4): 1–19, 2025. 2
- [28] Chandan Yeshwanth, Yueh-Cheng Liu, Matthias Nießner, and Angela Dai. Scannet++: A high-fidelity dataset of 3d indoor scenes. In *Proceedings of the IEEE/CVF International Conference on Computer Vision*, pages 12–22, 2023. 5
- [29] Hong-Xing Yu, Haoyi Duan, Charles Herrmann, William T Freeman, and Jiajun Wu. Wonderworld: Interactive 3d scene generation from a single image. In *Proceedings of the Computer Vision and Pattern Recognition Conference*, pages 5916–5926, 2025. 2
- [30] Junsheng Zhou, Yu-Shen Liu, and Zhizhong Han. Zero-shot scene reconstruction from single images with deep prior assembly. *Advances in Neural Information Processing Systems*, 37:39104–39127, 2024. 2
- [31] Xiaoyu Zhou, Xingjian Ran, Yajiao Xiong, Jinlin He, Zhiwei Lin, Yongtao Wang, Deqing Sun, and Ming-Hsuan Yang. Gala3d: Towards text-to-3d complex scene generation via layout-guided generative gaussian splatting. *arXiv preprint arXiv:2402.07207*, 2024. 2

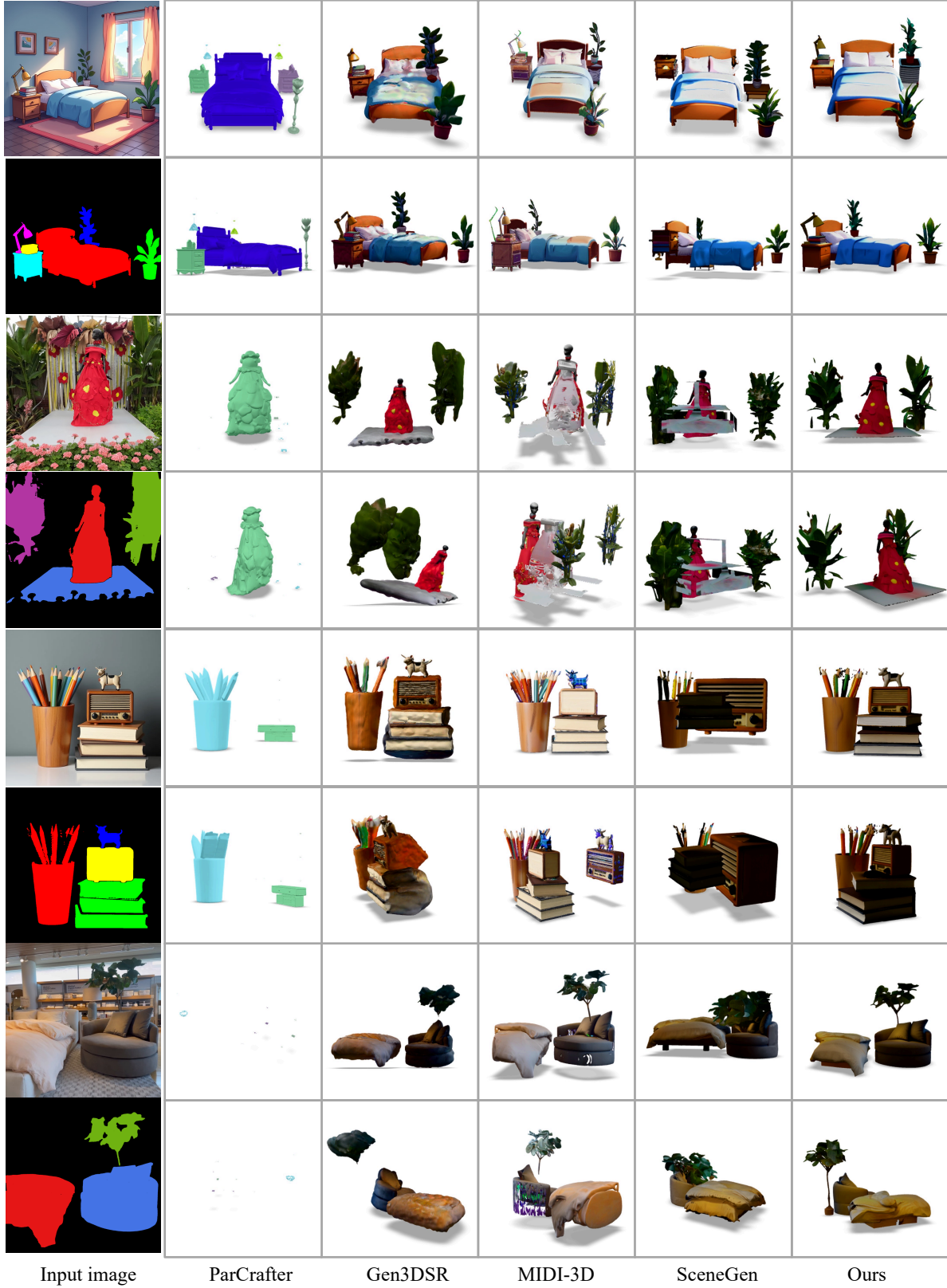


Figure 6. We present the multi-view evaluation results using real-world /stylized image as input (example 1). The testing scenes contain various layouts including *front*, *back*, *right*, *left*, *small on large*, *behind*, and etc. Baselines includes PartCrafter [13], Gen3DSR [1], MIDI-3D [8], and SceneGen [17]

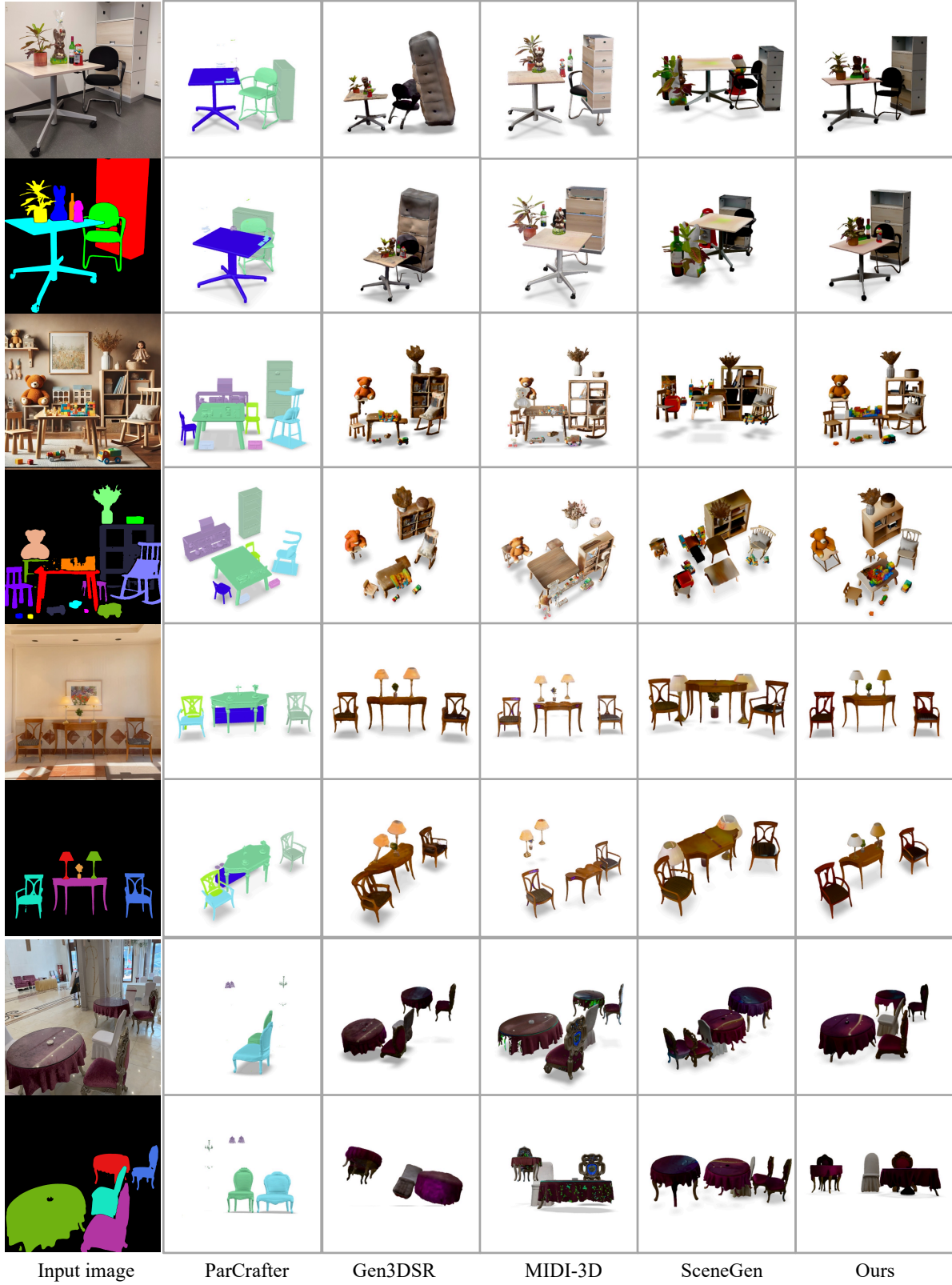


Figure 7. We present the multi-view evaluation results using real-world /stylized image as input (example 2). The testing scenes contain various layouts including *front*, *back*, *right*, *left*, *small on large*, *behind*, and etc. Baselines includes PartCrafter [13], Gen3DSR [1], MIDI-3D [8], and SceneGen [17]

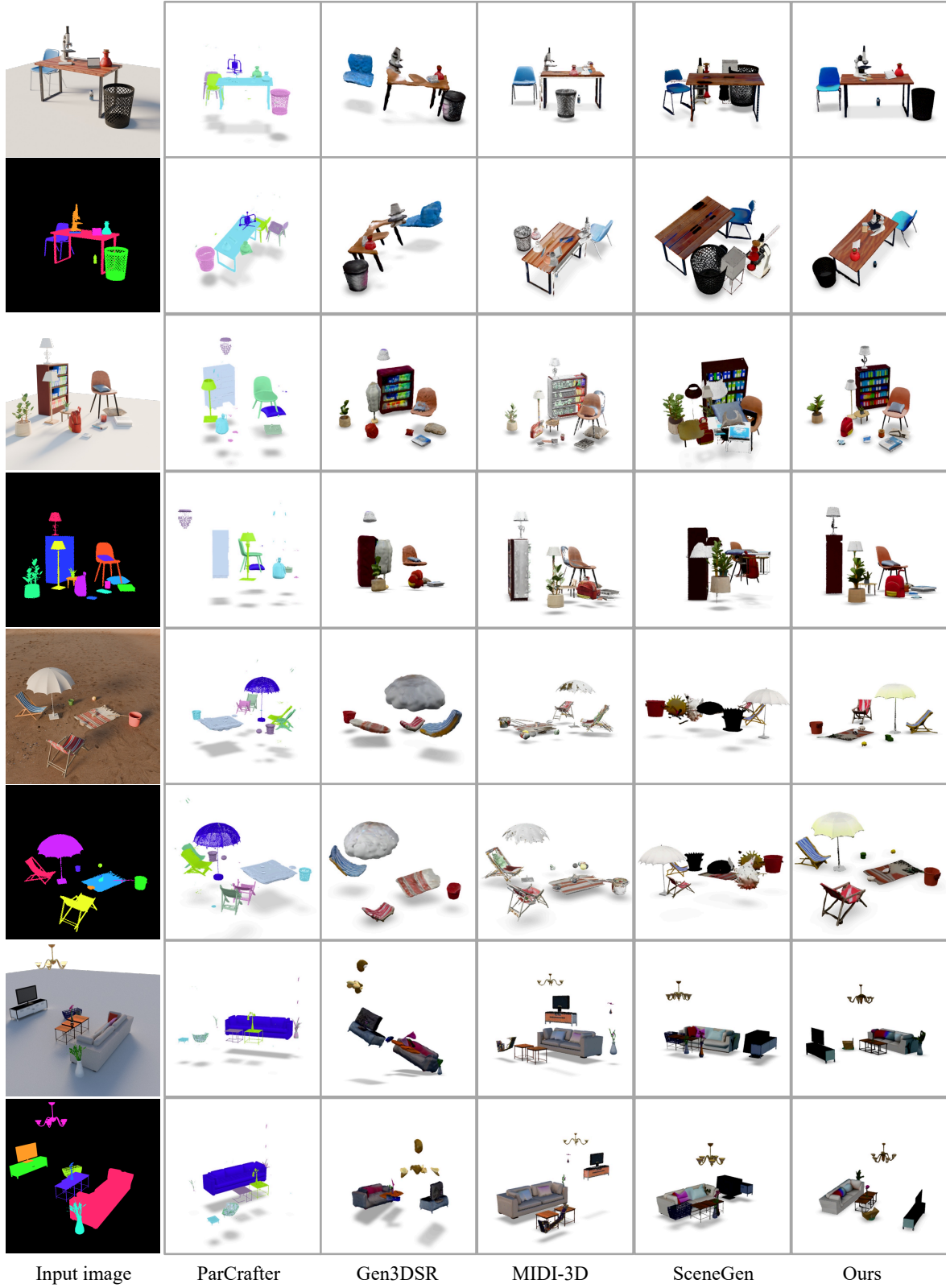


Figure 8. We present the multi-view evaluation results using synthetic scenes as input. The testing scenes contain various layouts including *front*, *back*, *right*, *left*, *small on large*, *behind*, and etc. Baselines includes PartCrafter [13], Gen3DSR [1], MIDI-3D [8], and SceneGen [17]



Figure 9. Ablation study on scene-context attention (SCA), view-centric space (VC), and non-semantic scenes (NS). With only SCA, the model often fails to maintain a coherent global layout and produces frequent object collisions. Adding the VC component substantially improves the overall arrangement of objects, but instance quality remains limited, as seen in the distorted cat, cow, and the chair under the toy bear. Incorporating NS further enhances both instance fidelity and global layout coherence.

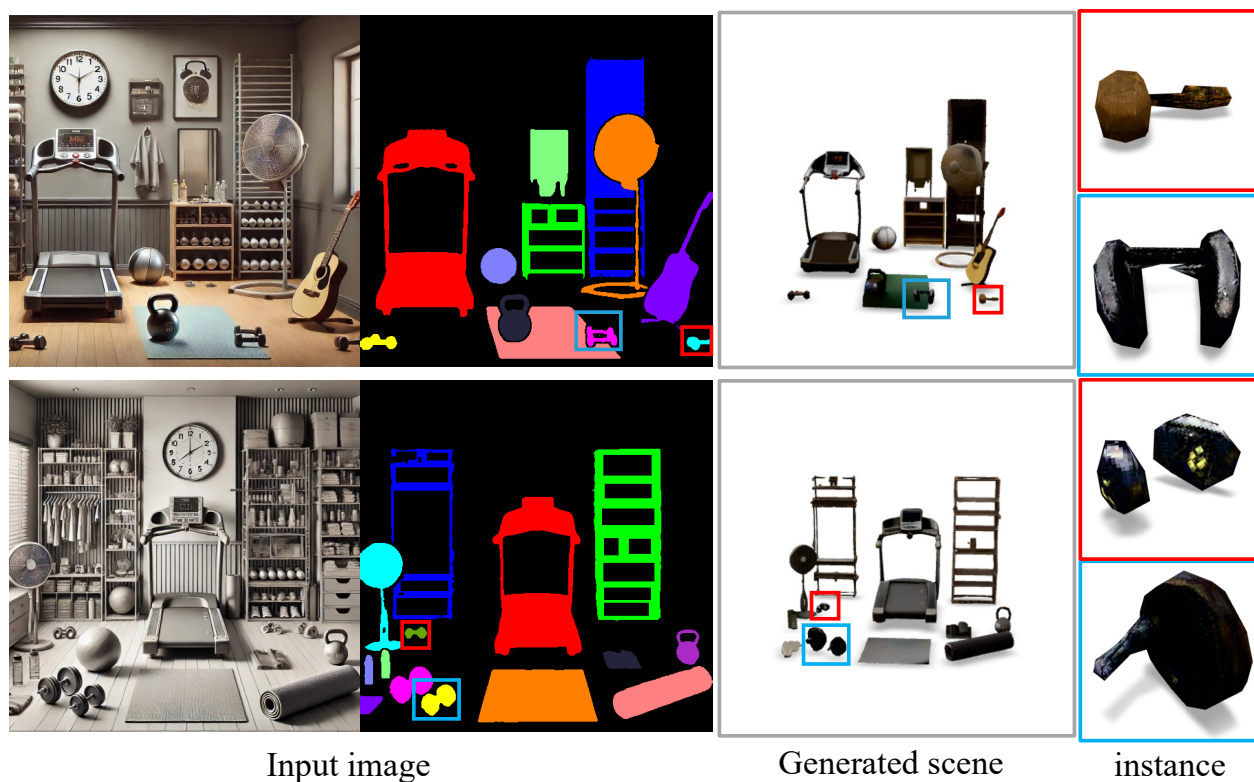


Figure 10. instance quality is bad when the input instance mask is small in the image.